Mountain-Top-to-Mountain-Top Optical Link Demonstration: Part II

A. Biswas[1] and M. W. Wright[1]

A mountain-top-to-mountain-top optical communications demonstration was conducted between the JPL Table Mountain Facility (TMF), Wrightwood, California, and Strawberry Peak (SP), Lake Arrowhead, California, during the months of August and September of 2000. The link was nearly horizontal at an altitude of 2 km and spanned a range of 46.8 km. A 780-nm multibeam beacon broadcast from TMF was received by the JPL Optical Communications Demonstrator (OCD) located at SP. The received beacon was utilized as a pointing reference to retransmit an 852-nm communications laser beam, modulated at 400 Mb/s by a PN7 pseudo-random bit stream (PRBS) sequence. The long atmospheric path resulted in atmospheric-turbulence-induced angle-of-arrival fluctuations of the beacon at the OCD aperture. A fine-steering control loop was used to track the resulting beacon centroid motion and update the pointing of the communications laser beam transmitted from SP to TMF. Fried parameters, or r_0, inferred from focal spot sizes received at SP were 4 to 5 cm whereas, using the spot sizes received at TMF, they were 2 to 3 cm. In both cases, theory predicts larger r_0 values. The predicted angle-of-arrival fluctuations compare well with measured rms displacements exhibited by the focal spots at either end of the link. An uncompensated error of ∼1.1 μrad in the x-axis and ∼2 μrad in the y-axis was obtained using centroid data logged by the OCD. Average bit-error rates of 10^{-5} were recorded for extended periods of time.

I. Introduction

This article is the second of two discussing results of an optical link demonstration conducted during August and September of 2000 between Strawberry Peak (SP), Lake Arrowhead, California, and JPL's Table Mountain Facility (TMF) in Wrightwood, California [1]. The link range was 46.8 km of a near-horizontal atmospheric path elevated approximately 2 km above the mean sea level. The first article emphasized the characterization of atmospheric-turbulence-induced scintillation over the horizontal path and the effectiveness of mitigation strategies at either end of the bidirectional laser link. The current follow-on article describes test results obtained with the NASA-patented Optical Communications Demonstrator (OCD) [2–4]. This includes an evaluation of the beacon irradiance fluctuations sensed by the OCD tracking sensor and the fine-tracking-loop performance of the OCD in responding to the atmospheric-turbulence-induced angle-of-arrival fluctuations of the received beacon. Finally, the

[1] Communications Systems and Research Section.

The research described in this publication was carried out by the Jet Propulsion Laboratory, California Institute of Technology, under a contract with the National Aeronautics and Space Administration.

end-to-end communications performance is evaluated by measuring the bit-error rates (BERs) for the 400-Mb/s PN7 pseudo-random bit stream (PRBS) sequence transmitted from SP.

The OCD was designed as a laboratory prototype of a space-based optical communications terminal. In the tests to be described, the OCD aperture is exposed to the atmosphere, a situation that deviates from expected space-flight scenarios. Nevertheless, the horizontal-path testing does provide an early cost-effective validation of the technology for future air- and space-borne flight communications. Both the laser beams received and transmitted by the OCD are subjected to atmospheric turbulence and the associated random refractive index perturbations.

Section II briefly discusses some of the atmospheric channel effects not discussed in Part I [1]. A brief discussion of the procedure to acquire data is provided in Section III. Results, including comparisons with theoretical predictions, are provided in Section IV, followed by conclusions in Section V.

II. Theory

The atmospheric scintillation effects and the resulting fade statistics were discussed in detail in Part I, and results were shown to validate a lognormal model. In the next section, results will be presented to show how the OCD tracking sensor performed in the presence of atmospheric scintillation.

The beam arriving at the aperture of the receiver exhibits angle-of-arrival fluctuations that translate to spot motion or "image dancing" at the focal plane. Defining the link range as L and the wave number of the laser beam as $k = 2\pi/\lambda$, λ being the laser wavelength, the parameter $\sqrt{L/k}$ for either end of the link is 0.0058 ($\lambda = 780$ nm) and 0.0063 ($\lambda = 852$ nm) and is much smaller than D, the receiving aperture diameter. Theory suggests that as long as $\sqrt{L/k} << D$, the angle-of-arrival fluctuations for a plane, spherical, and Gaussian beam wave are given by [5]

$$\sigma_\beta^2 = 2.914 C_n^2 L D^{-(1/3)} \tag{1a}$$

$$\sigma_\beta^2 = 1.093 C_n^2 L D^{-(1/3)} \tag{1b}$$

$$\sigma_\beta^2 \cong 1.093 C_n^2 L D^{-(1/3)} \left[a + 0.618 \Lambda^{11/6} \left(\frac{kD^2}{L} \right)^{1/3} \right] \tag{1c}$$

where σ_β^2 is the variance of the angle of arrival, C_n^2 is the atmospheric structure function, Λ and Θ are both output plane Gaussian beam parameters, and $a = (1 - \Theta^{8/3}/(1 - \Theta)$. Furthermore, $\Lambda = 2L/kW^2$ and $\Theta = 1 + (L/F)$, with W and F being the beam radius and phase front radius of curvature at the receiver. Equations (1a) through (1c) were derived for weak fluctuation theory but are also valid in the strong turbulence regime. Multiplying σ_β by the focal length of the receiving system yields the rms spot displacement at the focal plane. Using the OCD focal length of 2 m, the rms displacement for the plane wave case is 7.8 to 10.8 μm whereas, for the spherical and Gaussian beam wave, it is 4.8 to 6.6 μm. A similar prediction of rms displacement at the TMF receiver focal plane translates to 15 to 25 μm.

Atmospheric "seeing" effects contribute to enlargement of the received focal spot diameter. The effective spot size can be conceived of as being limited by an aperture that is the size of the atmospheric coherence length, r_0. Instead of a focal spot size given by $2.44 f\lambda/D$ (in the absence of atmosphere) for an incoming plane wave, the spot size increases to $2.44 f\lambda/r_0$, assuming $D > r_0$. The r_0 values for a Gaussian beam are predicted in the literature [5]:

$$r_0 = \left[\frac{8}{3(a + 0.618\Lambda^{11/6})}\right]^{3/5} (3.1 C_n^2 k^2 L)^{-(3/5)} \tag{2a}$$

For a plane and spherical wave, this relationship reduces to [5]

$$r_0 = (3.44 C_n^2 k^2 L)^{-(3/5)} \tag{2b}$$

$$r_0 = (1.16 C_n^2 k^2 L)^{-(3/5)} \tag{2c}$$

All of the above equations assume that $r_0 >> \ell_0$, the inner atmospheric scale. Substituting for C_n^2, k^2 and L in Eq. (2) yield theoretical r_0 values of 5.2 to 7.6 cm at SP and 5.7 to 8.5 cm at TMF for the plane-wave approximation. The theoretical r_0 values are defined as the $1/e$ radius of the atmospheric coherence. The r_0 values for the Gaussian- and spherical-wave cases are identical and from 9.3 to 13.7 cm at SP and 10 to 15 cm at TMF. Note that the range of r_0 values presented was computed for C_n^2 ranging between 10^{-16} and 5.2×10^{-17} m$^{-2/3}$. From these predicted estimates of r_0, the blurring of the spot size received by the OCD should be no more than a factor of 2 since the maximum bound on D/r_0 is $\sim$2. However, for TMF this bound is a factor of 6.

The predicted estimates of beam-spot displacement and blurring provided in the discussion above apply to a single beam arriving at the aperture. At TMF this is true; however, at SP multiple beacon beams arrive. The maximum angular displacement of these beams at TMF is approximately 10 μrad, the same as the angular pixel resolution of the OCD tracking sensor, also approximately 10 μrad. So, the multiple beacon beams will not be resolved by the OCD tracking sensor, provided they are co-aligned. The angle-of-arrival fluctuation of all eight beams is expected to be random and out of phase. This will influence the observed spot displacement as well as contribute to some blurring of the focal spot on the OCD tracking sensor. The modeling of the multiple-beam effects on the spot size and motion has not been done.

The impact of blurring at the receiver focal plane must be accounted for by providing adequate detector size and a tracking mechanism that compensates the image dancing in the focal plane, thereby ensuring good overlap between the receiving detector and the signal focal spot. This is particularly important for very high data-rate links, where the required detector bandwidth limits the diameter due to capacitive effects.

III. Data Acquisition Procedure

A. OCD Beacon Reception

Alignment between the OCD and the TMF telescope is established following the procedure described in Section III of Part I [1]. The beacon laser received by the OCD is focused to a spot on the acquisition and tracking charge-coupled device (CCD) sensor. A small fraction of the laser beam transmitted by the OCD is redirected to also focus on the acquisition and tracking CCD sensor. For convenience, "beacon" and "laser" are used for referring to the received beacon (780-nm) and transmitted laser (852-nm) spots. The optical alignment of the OCD is internally adjusted in a manner that prevents the beacon and laser spots from overlapping. When the beacon and laser beams are perfectly co-aligned, they appear at unique locations on the CCD. The centroids associated with these spot locations are determined under controlled laboratory conditions and predefined (laser and beacon home positions) in the control software. A third fixed parameter is the fine-steering mirror digital-to-analog converted (DAC) value associated with the laser home position. These three parameters are fixed in the control software. During tracking, an error signal is generated based upon the difference between the instantaneous and home positions of the beacon. This error can be caused, for example, by spacecraft vibration and/or atmospheric-turbulence-induced

angle-of-arrival fluctuations. In our case, since the OCD is fixed, the latter contributes to beacon centroid motion. After appropriate filtering, the error signal is fed to the fine-steering mirror (FSM) whereupon the pointing of the transmitted laser is moved in order to compensate for instantaneous change in the beacon angle of arrival. Since a small fraction of the transmit laser is also focused on the tracking sensor, the FSM pointing updates are accompanied by centroid motions of this laser spot. The control software used to evaluate the performance of the servo fine-pointing loop utilizes a CCD frame update rate of 1 kHz. A graphical user interface (GUI) allows activation of the acquisition mode during which 10-second segments of beacon intensity and x- and y-centroid are logged continuously. The intensity is related to the aggregate counts of a 10×10 sub-window enclosing the spot. For centroiding, a real-time background subtraction method is used, allowing the processing of faint beacon signals reliably. In the tracking mode, 5-second segments of spot intensities and x- and y-centroids of both beacon and laser are logged.

B. Beacon Spot Size and Intensity

By simultaneously monitoring the beacon signal through the spotting telescopes described in Part I, the incident irradiance at SP (also the OCD aperture) was determined to be approximately 0.1 nW/cm^2. The incoming beacon irradiance was adjusted to this level by adding neutral density filters to the beacon transmit optical train at TMF. The choice of irradiance level is dictated by CCD exposure time, spot size, noise floor, and the saturation level. For the OCD's tracking loop to work properly, the beacon fades and surges have to be minimized. In the present stage of development, the control-loop software is not tolerant to fades, while centroiding accuracy depends on the extent of saturation introduced by surges. For example, if a surge causes "blooming" of the CCD, then a reliable centroid cannot be computed; on the other hand, a single pixel saturating does not introduce too much centroiding error. The CCD signal in response to the incident beacon spot is effectively the integrated pixel count over background. The incoming mean irradiance needs to match a CCD signal that is suitably positioned above the noise floor so that the atmospheric fades result in acceptable signal-to-noise ratios. This was determined by visually minimizing fades in the beacon spot displayed on the GUI. Ideally, both fades and surges are to be avoided in order to facilitate the best centroiding accuracy; however, the CCD on the OCD has a limited dynamic range, and during the demonstration surges that caused saturation of a few pixels without causing blooming were tolerated, while attempts were made to completely eliminate fades.

IV. Results and Discussions

A. Received Focal Spot Size

As discussed earlier in Section II, the focal spot on the OCD tracking sensor is subject to atmospheric-seeing-induced distortions. Individual image frames were stored in order to examine the beacon spot. Figure 1(a) shows a typical OCD tracking sensor frame image. As described in Section III.A, two spots are incident upon the focal-plane CCD sensor. The spot associated with the beacon laser [upper left in Fig. 1(a)] that has traversed an atmospheric path displays blurring due to atmospheric seeing effects. After processing 20 images acquired at various times during the night of August 4, it was determined that beacon spot sizes typically varied between 5×5 and 7×7 pixels, compared to the 3×3 to 4×4 spot sizes without atmospheric seeing effects (laboratory results). If the spot sizes measured were related to $(2.44 f \lambda)/r_0$, where f and λ represent the focal length and wavelength and r_0 is the atmospheric coherence length, then r_0 values of 3 to 5 cm can be inferred. The inferred r_0 value is smaller than the 5- to 7-cm value predicted for a plane-wave model, as well as the 9 to 13 cm predicted for Gaussian- and spherical-wave models. Note that r_0 and spot size are inversely related. Therefore, the larger than predicted spot size observed may be due to the use of a multibeam beacon where imperfect alignment between the incoming beams would contribute to additional spreading of the focal spot. This is merely conjecture since sufficient analysis and controlled experiments have not been carried out to prove this conclusively.

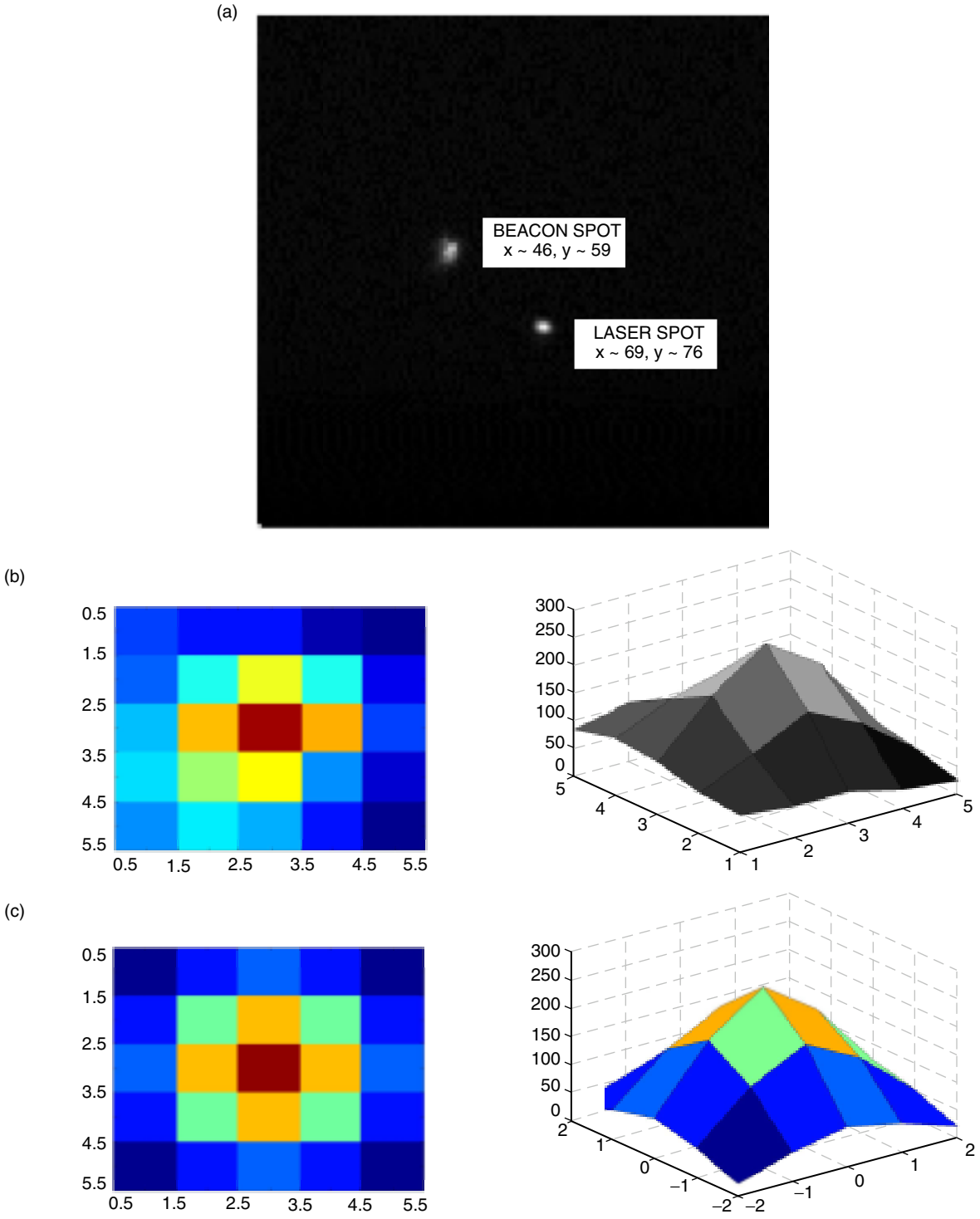

Fig. 1. Beacon spot size incident on the tracking focal-plane array: (a) a typical image frame of the OCD tracking sensor where the enlarged spot size of the beacon is due to atmospheric seeing effects; the laser spot that does not traverse an atmospheric path serves as a reference of what the spot would appear like without the blurring effects, (b) a contour and surface plot of a typical beacon spot enclosed in a 10-by-10 pixel sub-frame, and (c) a simulation of a perfect Gaussian spot. Comparison of Figs. 1(b) and 1(c) shows that the beacon spot is not subjected to severe degradation because the OCD collecting aperture is approximately 2 times the atmospheric coherence length, causing mostly shifts in the spot location.

The focal spot beam profile was examined, with a typical example shown in Fig. 1(b). For comparison, Fig. 1(c) shows the beam profile for an ideal Gaussian beam. The extent of distortion determined by comparison in a qualitative sense is not too severe, and this supports the premise that the aperture size is approximately 2 to 3 times r_0, limiting the number of competing modes and, hence, the beam profile.

B. Received Beacon Power and OCD Centroiding

The OCD fade threshold is determined by the minimum aggregate counts measured over the framing sub-window used for centroiding. It was observed that, for aggregate pixel counts of less than 200 and using a 10×10 pixel sub-window, the centroiding failed. Instances of the centroiding failing were very rare and were encountered on a few frames (less than 10) for 2 of the 22 data sequences logged. This suggests that the approach used to eliminate beacon fades, namely, setting the beacon irradiance to a level where the minimum signal could be sensed while allowing CCD pixels to saturate during irradiance surges, was effective. Post-processing of acquired image files of the beacon spot [Fig. 1(a)] indicates that at approximately 500 to 800 aggregate counts the noise floor of the CCD sensor is encountered; however, the centroiding algorithm continues to extract position information by performing background subtraction. Given these observed characteristics of the CCD sensor, we can conclude that nearly all the data logged in August and September were fade free. Note that this is true in spite of the fact that the CCD sensor dynamic range was only 7 dB.

On the other hand, approximately 3200 counts correspond to the brightest pixel of the focal spot saturating, while 3200 to 5500 counts represent 4 to 5 saturated pixels and, above 5500 counts, blooming of pixels is encountered. Figure 2 shows two typical cumulative density functions (CDFs) of beacon spot intensity as recorded in terms of aggregate pixel counts for the 10×10 centroiding frame of the CCD. The two CDFs represent different mean signal levels, also indicated in Fig. 2. The OCD noise threshold and different pixel saturation levels as determined by studying beacon spot images are also annotated on the CDFs. Thus, in Fig. 2(a), the mean beacon intensity of 2232 counts avoids blooming and excessive saturation while, on the other hand, in Fig. 2(b) a mean beacon intensity of about 3500 counts represents a large fraction of the received spots undergoing saturation on a significant fraction of the illuminated pixels, and, as will be shown below, this gives rise to increased tracking errors. As Fig. 2 shows, the true dynamic range of the CCD extending from the minimum beacon spot intensity sensed (∼600 counts) until a pixel starts saturating (∼3000 counts) is ∼7 dB. In spite of this limited dynamic range, the fact

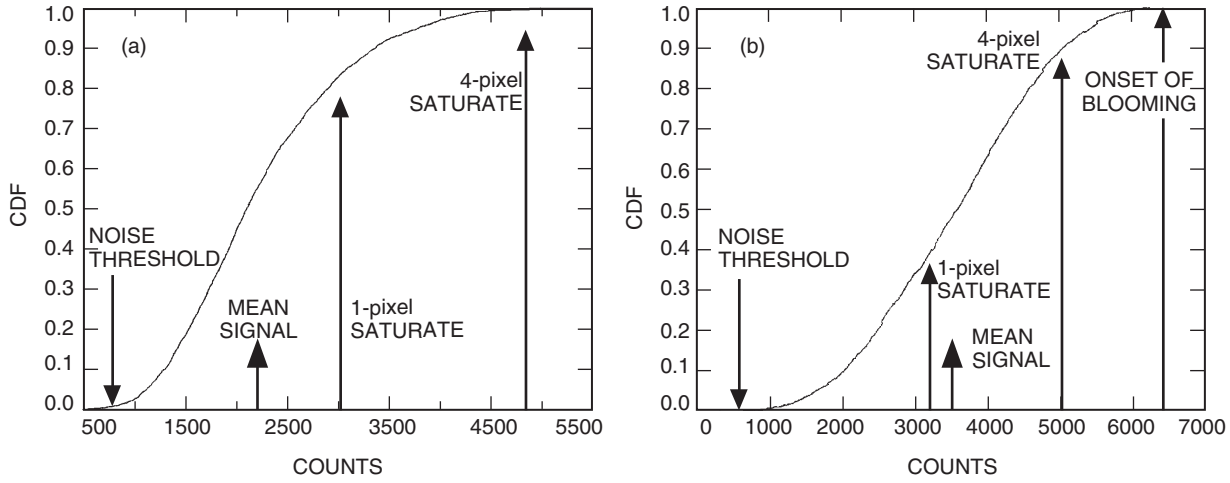

Fig. 2. Cumulative density function for a beacon spot intensity (sum of illuminated pixel counts) recorded by the OCD for a mean signal of (a) 2232 counts and (b) 3521 counts. The distribution represented by Fig. 2(a) is favored because lower centroiding errors will be incurred.

that beacon irradiances were adjusted to allow a certain amount of saturation while sensing the minimum irradiance allowed the fade-free operation asserted above. As shown below, operating at mean irradiance levels represented by Fig. 2(b) as opposed to those shown in Fig. 2(a) resulted in loss of performance even though fades were eliminated. The control-loop algorithm used was not fade tolerant.

The mean and standard deviations of the measured CCD signal were used to determine the normalized variance or scintillation index (SI). Since simultaneous data acquisitions were made while receiving the beacon with the OCD and the spotting telescopes, a comparison of the SI determined from the spotting telescope data (reported in Part I) and from the CCD signal was made. Table 1 shows this comparison. Allowing for some margin of uncertainty in the measurements, the OCD appears to consistently record a lower SI value. The factor of 2 differences in sampling rates used [1 kHz for the CCD and 2 kHz for the avalanche photodiode (APD) does not explain this observation. This was verified by using a 2-point averaging of the APD data and determining that the decrease in SI never exceeds 3 percent, whereas much larger differences are observed in Table 1. Closer examination shows that the difference in APD- and CCD-measured SI values is correlated to the mean signal count level logged on the CCD. If the mean signal count sensed by the CCD is too close to either the noise floor or the pixel saturation level, the variance of the intensity is not properly tracked due to "clipping," causing the normalized variance to appear smaller. On the other hand, if the mean signal level is positioned properly between the noise floor and saturation ceiling, then the true extent of signal fluctuation is sensed. Figure 3 illustrates this for two simultaneously acquired (APD and CCD) data sets, where in one case the mean counts are roughly 2200 and in the other about 3500. The former data set shows lognormal intensity distributions for both APD and CCD data; however, the CCD measurement for the second data set is plagued by saturation effects, making the intensity distribution appear normal by clipping (suppressing) the larger intensity values. The APD data that do not suffer from this artifact indicate the expected lognormal distribution. The true extent of the fluctuation of the beacon laser is suppressed by the OCD unless the mean irradiance matches a suitable signal level; as will be shown below, the suppression of the true extent of the fluctuation results in a penalty in tracking performance.

Table 1. Comparison of SIs obtained from simultaneous acquisitions on the OCD and the spotting telescopes.

CCD	APD
0.14	0.25
0.43	0.41
0.11	0.15
0.13	0.17
0.13	0.19
0.08	0.21
0.15	0.13
0.12	0.17
0.11	0.23
0.10	0.26
0.12	0.33
0.22	0.41
0.28	0.40

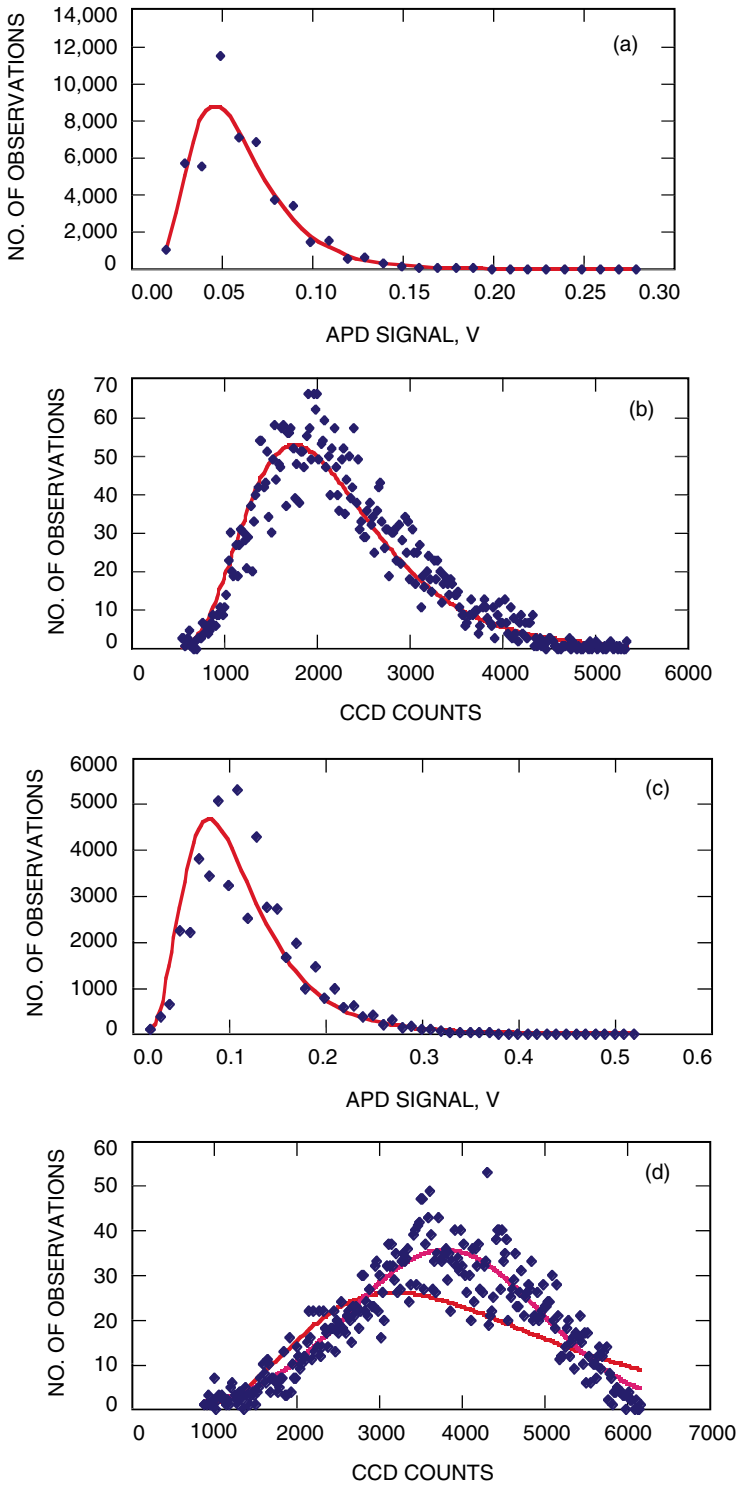

Fig. 3. Intensity distributions using (a) an APD and (b) a CCD fitted to a lognormal distribution (the mean CCD signal is 2200 counts), and a second data set showing (c) APD- and (d) CCD-measured intensity distributions (when the mean CCD counts are 3500); in this case, the CCD pixel saturation caused the intensity distribution to appear like a normal rather than a lognormal distribution.

C. Tracking Performance

1. Open-Loop Tracking. Data logged by the OCD during beacon acquisition provide an indication of the extent of beacon centroid motion. Figures 4(a) and 4(b) show a typical distribution of x- and y-centroid values in pixel units for a 5-second acquisition of the beacon. The distribution of centroids fits a normal distribution, corroborating the random nature of the angle-of-arrival fluctuations. Using the fit, the rms displacement can be determined, as was done for all the data sets. Figures 4(c) and (d) show histograms of the rms displacement (in micrometers) observed over the course of our demonstration that includes measurements made during the nights of August 4 and September 13 through 15. The y-centroid exhibits a larger displacement, and this is an artifact of the CCD read-out that exhibits sporadic skips in reading out lines. Therefore, the x-values are more representative. Thus, the 7.8- to 11-μm predicted theoretical value (see Subsection II.A) is reasonably well supported by the observed distribution of displacements centered around 9 to 11 μm in Fig. 4(c). It is also noteworthy once again that the spherical- and Gaussian-wave-model-predicted rms displacement of 5 to 7 μm is definitely lower than the observed extent. In making these comparisons, angle-of-arrival variation introduced by beam

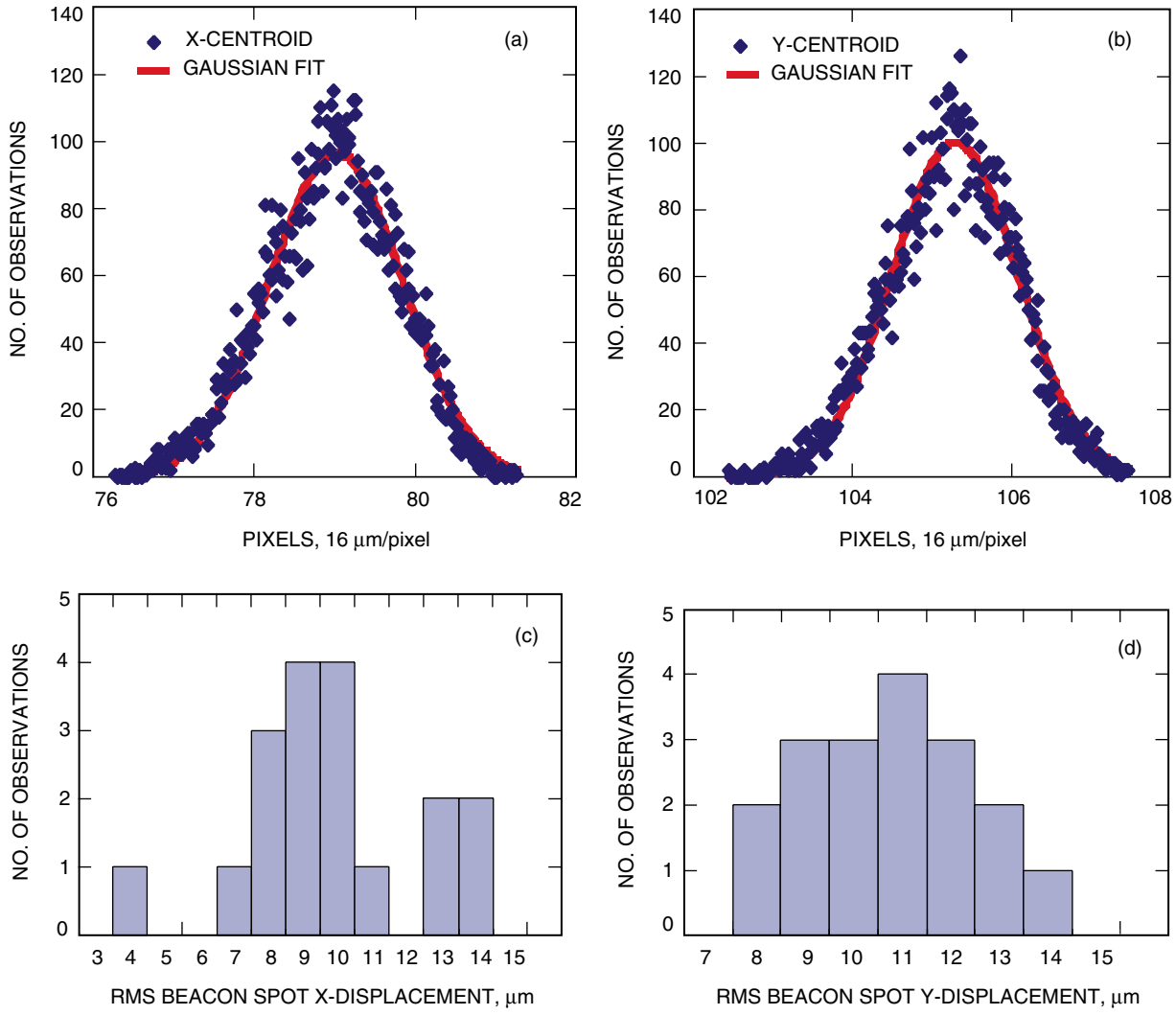

Fig. 4. The typical distribution of (a) x-centroids and (b) y-centroids in pixel units for the beacon spot incident upon the OCD (the distribution of centroids is a result of angle-of-arrival fluctuations experienced by the beacon traversing 46.8 km of atmosphere), and histograms of the rms (c) x-displacement and (d) y-displacement in µm of the beacon spot for measurements made on the nights of August 4 and September 13, 14, and 15, 2000.

wander that is a refractive bending of the laser beam is being ignored; this is a much lower frequency occurrence and, over the data acquisition time of 5 seconds, would induce a very slight drift in mean angel of arrival. From the data, no such effect can be clearly identified.

Furthermore, the rms beam displacement also applies to a single beam arriving at the OCD aperture, whereas in our demonstration there are 8 nominally co-aligned beams arriving. The data, however, can be satisfactorily explained by assuming a single beam arriving at the aperture. This would once again suggest that the intra-beam angular displacement is below the resolution of the OCD pixels.

Both the rms angle-of-arrival and the r_0 values inferred from the data gathered by the OCD suggest a better fit to a plane-wave model. Yet in Part I, the SI measurements were observed to better fit the saturation model for a spherical- or Gaussian-wave model. Since measurements with the OCD on single-beacon beams were not made, we merely note this fact.

2. Closed-Loop Tracking. Figure 5(a) shows a 1-second duration of recorded beacon- and transmit-reference laser-spot centroids recorded by the OCD. As expected, the displacement of the beacon centroid

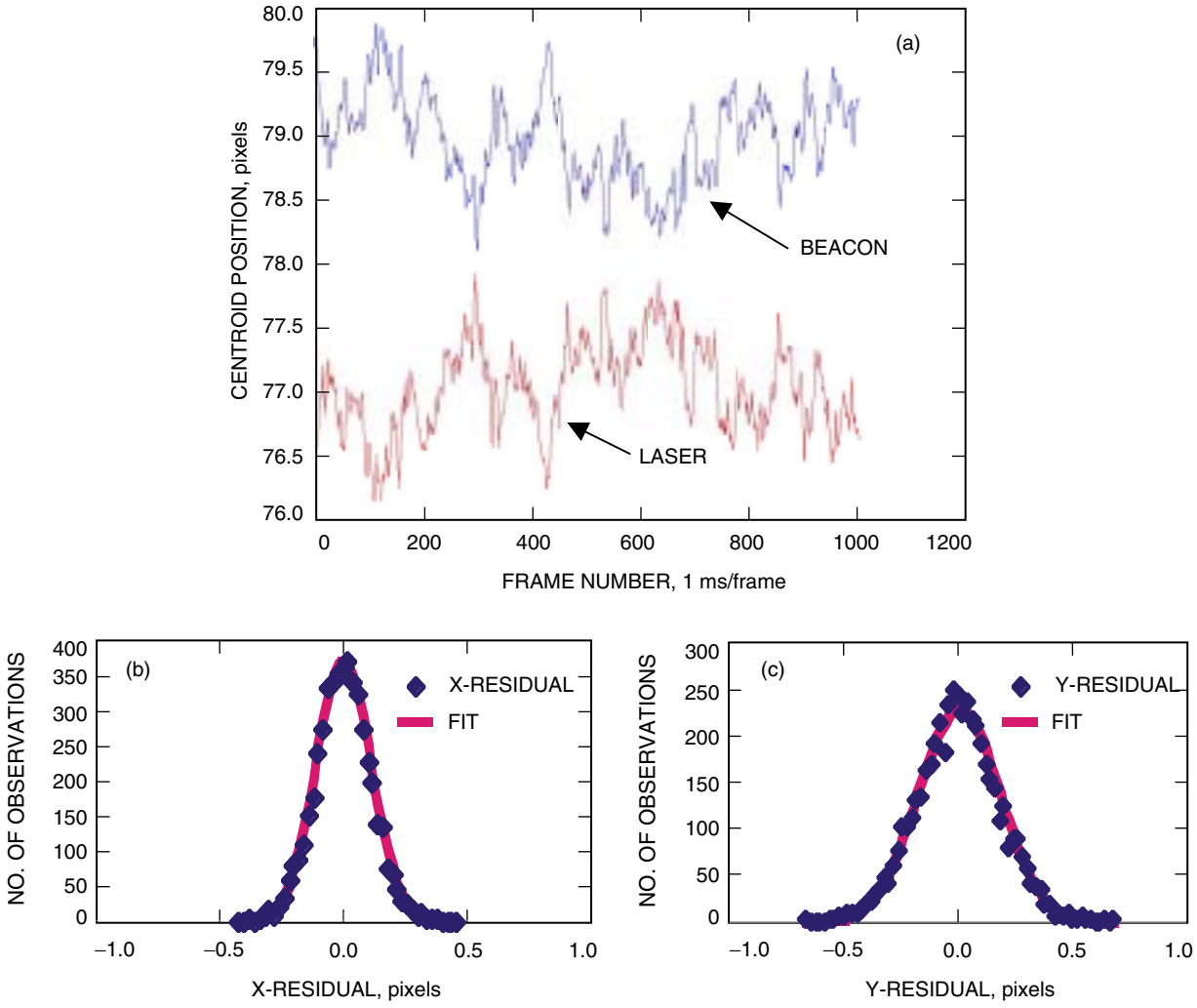

Fig. 5. Summary of fine tracking data obtained using the OCD over the 45-km horizontal-path optical link: (a) a time series of the beacon x-centroid position varying due to atmospheric perturbation alongside the laser x-centroid position that is being updated by the fine-steering loop in response to the motion of the beacon, and histograms of the residual error in the (b) x-direction and (c) y-direction.

is compensated by a corresponding oppositely directed motion of the transmit reference spot due to an update of the fine-steering mirror. This compensation should point back the OCD laser to the location from which the beacon appears to have arrived, thus compensating for the angle-of-arrival fluctuations caused by atmospheric turbulence. The nature of the OCD tracking loop is such that, in response to any beacon motion, the transmit-reference laser spot moves in the opposite direction on the tracking sensor, so that adding the incremental changes in the x- and y-directions should cancel out exactly. However, imperfect loop performance results in some residual error. Figures 5(b) and 5(c) show histograms of the residual x- and y-motion resulting from summing the incremental x- and y-motion for each frame of data recorded.

The histograms in Figs. 5(b) and 5(c), fitted to a Gaussian distribution, represent the rms residual error; determined from the fits, these are ± 0.1035 and ± 0.1652 pixels in the x- and y-directions, respectively. The larger value in the y-direction is attributed once again to the previously mentioned artifact of the CCD read-out. Based on the plate scale of the OCD, this corresponds to ± 1.0 and ± 1.7 μrad of uncompensated error. The data presented in Figs. 5(b) and 5(c) represent the best tracking results obtained during our demonstration.

Figure 6 shows several residual error values plotted as a function of the mean received signal counts. This plot displays the range of residual error values in the x-direction (1 to 2.25 μrad) observed during the demonstration. The residual errors are related to the mean received signal. Larger aggregate counts result in increased centroiding error due to pixel saturation, as do smaller aggregate counts due to poor signal-to-noise ratio. For beacon intensities corresponding to approximately 2000 to 3000 counts, the best performance is apparent. A second-order polynomial fit to the data of Fig. 6 shows the trend.

The spot motions on the CCD can also be described by the power spectral densities (PSDs). Figure 7 shows PSDs for the x- and y-centroid motion. For comparison, Fig. 7(a) also includes Olympus spacecraft vibration PSDs [6] that indicate the beacon motion induced by atmospheric turbulence across the horizontal range is comparable to spacecraft jitter typically used to validate fine-tracking performance of optical communications terminals.

The OCD fine-steering control loop was independently characterized [7] in the laboratory using the upgraded fine-steering mirror, and the derived model is shown in Fig. 7(b), where the control-loop bandwidth is close to 70 Hz. The rms residual motion can be determined using the relationship

$$\theta_{\mathrm{rms}} = \sqrt{\int S(f)\,|R(f)|^2 df} \tag{3}$$

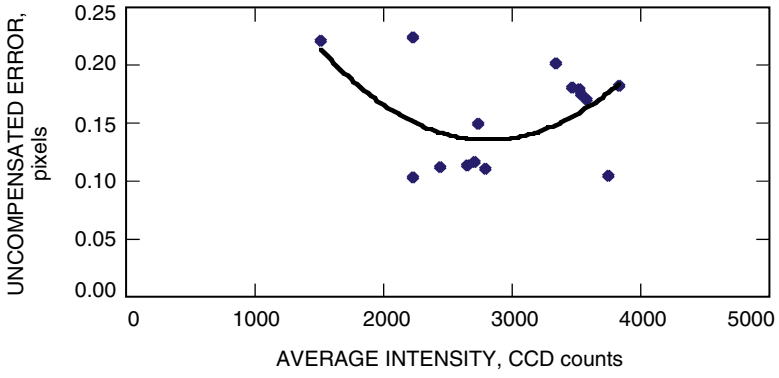

Fig. 6. The correlation between the mean beacon intensity sensed by the CCD tracking sensor and the uncompensated error. The minimum uncompensated error corresponds to a mean beacon intensity between 2000 and 3000 counts.

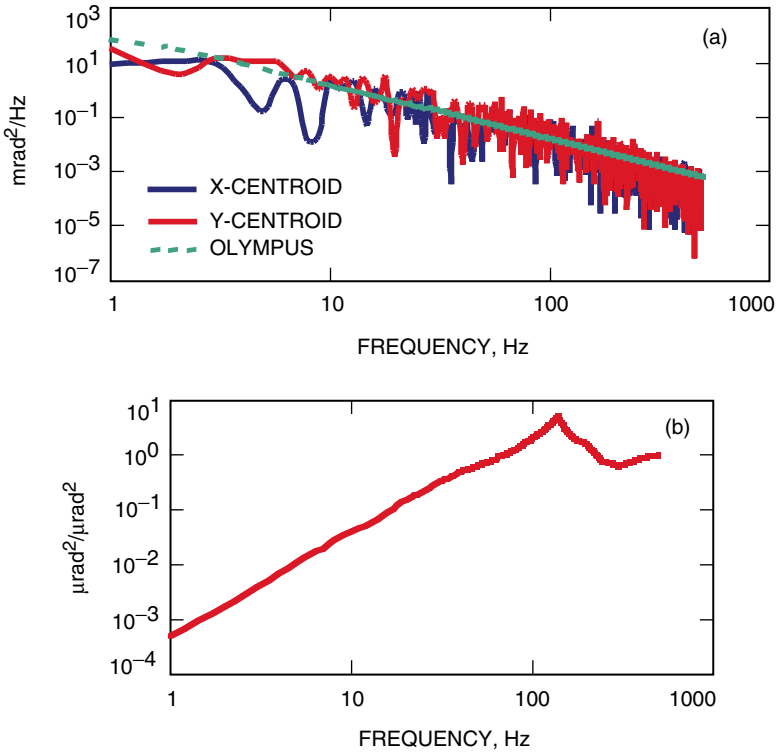

Fig. 7. Injected disturbance and control-loop rejection characteristics: (a) PSDs of beacon spot displacement caused by atmospheric-turbulence-induced angle-of-arrival fluctuation references to the PSD for the Olympus spacecraft vibrations and (b) the rejection function determined for the (Left Hand Design Inc. Model FO-15) fine-steering control loop.

where $S(f)$ is the angular-motion beacon power spectral density [Fig. 7(a)] derived from the centroid time series [Fig. 5(a)], and $R(f)$ is the tracking-control-loop rejection function [Fig. 7(b)]. The $\theta_{\rm rms}$ determined using Eq. (3) was 3.4 μrad. The determination of $\theta_{\rm rms}$ is worse than the 1.1 to 2.3 μrad obtained by making a direct comparison between the time series of the beacon and laser spot centroids logged by the OCD.

D. TMF Spot-Size Characteristics

The scintillation index of the received communications laser signal measured at TMF was presented in Part I. The spot size received at TMF was examined using a CCD camera. Even though the frame update rate of the CCD was 30 Hz, the exposure time was reduced to 1/1000 of a second using an electronic shutter. Figure 8 shows a histogram of the spot diameter required to enclose about 87 percent of the received energy at the focal plane. The measured mean spot diameter lies between 300 and 400 μm. The spot size measured at TMF utilized a lens with an effective focal ratio of 8, whereas the 60-cm telescope focal ratio was 41. Therefore, the spot size at the Coudé focus can be estimated to be 2.3 mm in diameter. Approximating spot diameter at the Coudé focus by $(2.44f\lambda/r_0)$ allows an inference of $r_0 = 2$ to 3 cm. The predicted value of r_0 in this case is significantly smaller than the prediction of 5.7 to 8.5 cm (see Section II).

The spot motion due to angle-of-arrival fluctuations at TMF was determined using centroiding of the spots; the distribution is shown in Fig. 9. The rms displacement was ± 58 μm compared to a predicted value [Eq. (6)] of ± 15 to 25 μm.

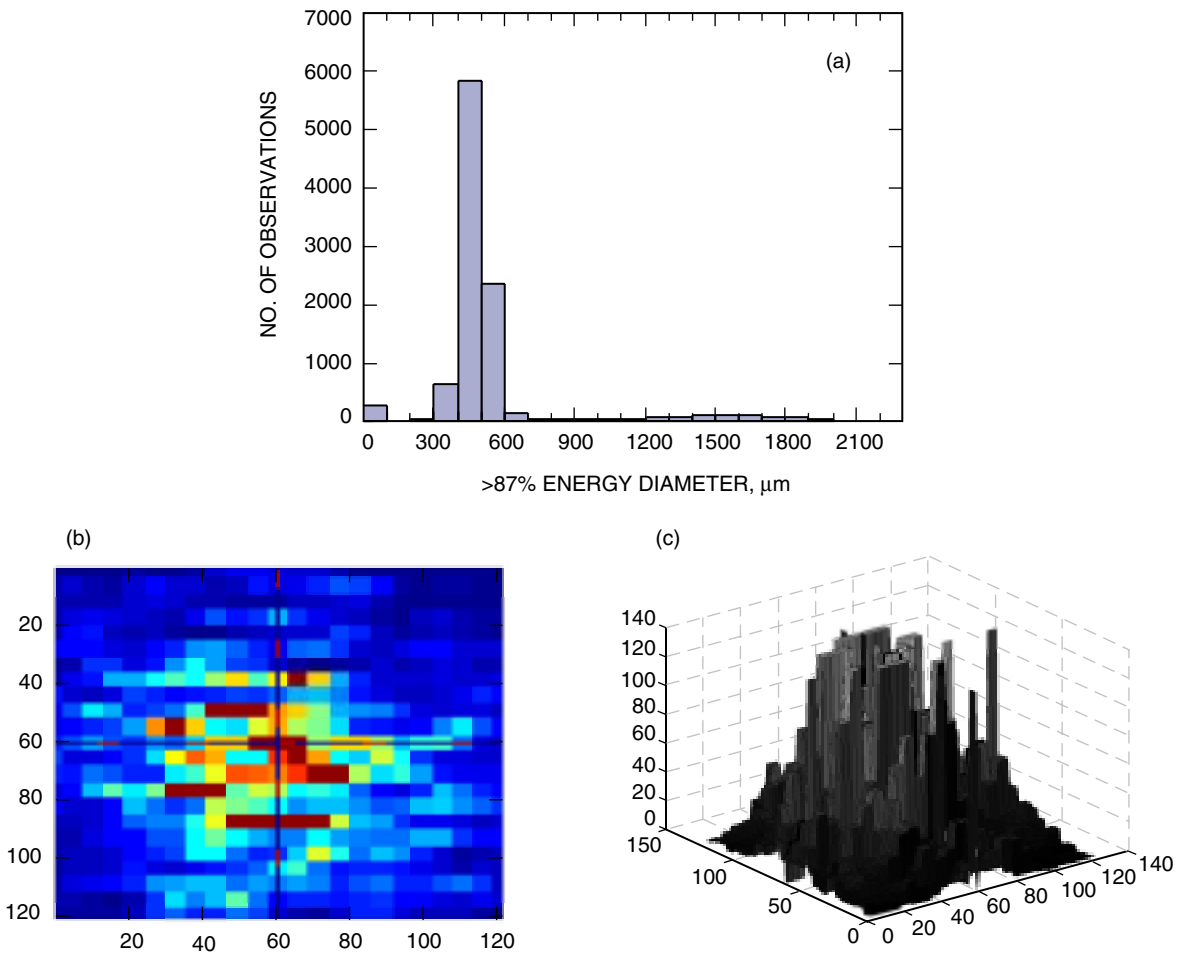

Fig. 8. Data gathered on the focal spot size received at TMF: (a) histogram of the spot-size (enclosing >897% energy) distributions, (b) appearance of a typical focal spot recorded by the CCD camera, and (c) a surface plot of the spot size recorded by the CCD camera.

E. Communications Performance

Satisfactory eye patterns were recorded at TMF, and a representative pattern captured from the oscilloscope is shown in Fig. 10(a). The eye patterns displayed were fairly typical and were obtained by feeding the recovered data and clock to the oscilloscope. The data rate used was 400 Mb/s, with pseudo-noise (PN7) encoded, on-off keyed (OOK), non-return to zero (NRZ) pseudo-random bit stream (PRBS). When connected to the receiver module of a bit-error-rate tester (BERT), the same signal recorded BER measurements with an update rate of 1 second. Figure 10(b) represents some of the best results obtained on September 13, 2000. Typically, BERs between 10^{-4} and 10^{-5} were observed. These BERs represent a time average. Using an extended acquisition oscilloscope, a 2-ms sequence of bits was recorded and compared to the modulation signal. From this comparison, it is apparent that the optical communications system used is bandwidth-limited, giving rise to errors. The laser driver is the most likely element that is limiting the bandwidth. Unfortunately, the previously characterized laser driver intended for the demonstration failed, resulting in the adaptation of an untested laser driver and laser. Although this laser assembly was specified to be adequate for 500 Mb/s, it is apparent that the performance at 400 Mb/s is degraded due to bandwidth limitations. This appears to be limiting the bit-error-rate measurements.

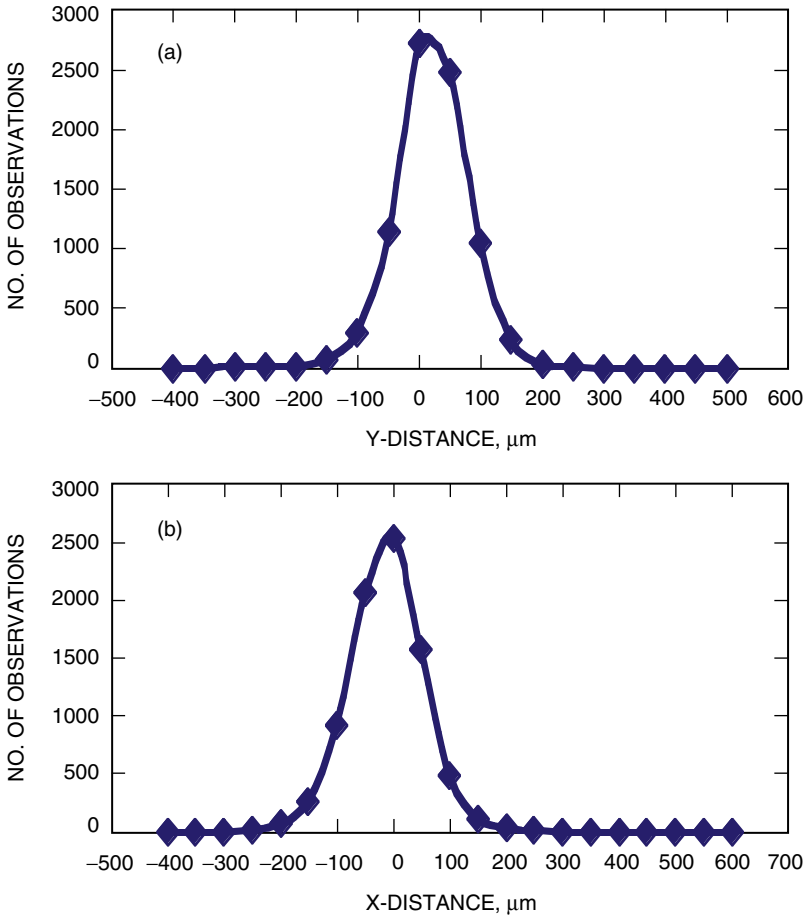

Fig. 9. The extent of spot centroid motion at the TMF focal plane in two orthogonal directions on the CCD sensor: (a) y-direction and (b) x-direction.

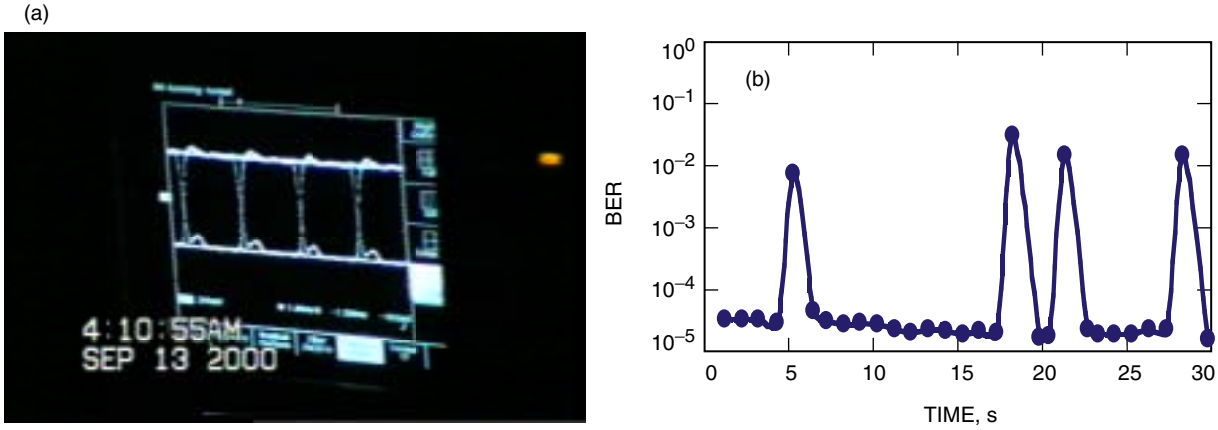

Fig. 10. The received communications signal transmitted by the OCD underwent clock and data recovery at TMF: (a) typical eye pattern recorded at TMF and (b) bit-error rate recorded by the bit-error-rate tester.

V. Conclusions

An atmospheric coherence length r_0 of 3 to 5 cm was inferred using the focal-plane spot size measured on the CCD tracking sensor and compared to a predicted value of 5 to 7 cm using reasonable atmospheric models. The irradiance bounds required for the CCD tracking sensor to perform centroiding was found to range from 2000 to 3000 integrated pixel counts, although a more reliable range was 600 to 3000, indicating a dynamic range of 6 to 11 dB. The motion of the spot on the focal plane was also recorded and yielded rms angle-of-arrival-induced focal-plane displacement of 9 to 11 μm, compared to a predicted value of 7.8 to 11 μm. The irradiance measurements made with the OCD clearly indicate that best tracking performance is obtained when the mean received signal is 2000 to 2200 counts. The best tracking performance resulted in an rms uncompensated error of ± 1.1 μrad. The uncompensated error appeared to increase with either an increase or decrease in mean beacon-signal level. The rms uncompensated error determined by deriving the beacon displacement power spectral density from the beacon centroid-versus-time data and the rejection function of the control loop yielded a higher value of 3.4 μrad.

The mean spot diameter measured at TMF for the communications beam was between 300 and 400 μm, suggesting r_0 values of 2 to 3 cm, compared to predicted values of 5.7 to 8.5 cm. The rms displacement due to angle-of-arrival fluctuations at TMF was measured to be ± 58 μm, compared to a predicted value of ± 15 to 25 μm. The lowest bit-error rates observed were 10^{-5} even though there was no evidence that the link was limited by atmospheric fades. The study of stored 2-ms-duration data sequences indicated poor laser-driver performance as a key contributing factor to the limited link performance.

References

[1] A. Biswas and M. W. Wright, "Mountain-Top-to-Mountain-Top Optical Link Demonstration: Part I," *The Interplanetary Network Progress Report 42-149, January–March 2002,* Jet Propulsion Laboratory, Pasadena, California, pp. 1–27, May 15, 2002.
http://ipnpr.jpl.nasa.gov/tmo/progress_report/42-149/149B.pdf

[2] J. Lesh, C.-C. Chen, and H. Ansari, "Lasercom System Architecture with Reduced Complexity," U.S. Patent Number 5,517,016, May 1996.

[3] M. Jeganathan, A. Portillo, C. S. Racho, S. Lee, D. M. Erickson, J. Depew, S. Monacos, and A. Biswas, "Lessons Learned from the Optical Communications Demonstrator (OCD)," *Free-Space Laser Communications Technologies XI, Proceedings of SPIE,* G. S. Mecherle, ed., vol. 3615, pp. 23–30, 1999.

[4] M. Jeganathan and S. Monacos, "Performance Analysis and Electronics Packaging of the Optical Communications Demonstrator," *Free-Space Laser Communications Technologies XI, Proceedings of SPIE,* G. S. Mecherle, ed., vol. 3226, p. 33, 1998.

[5] L. C. Andrews and R. L. Phillips, *Laser Beam Propagation through Random Media,* chs. 6 and 7, Bellingham, Washington: SPIE Optical Engineering Press, 1998.

[6] M. Wittig, L. van Holtz, D. E. L. Tunbridge, and H. C. Vermeulen, "In-Orbit Measurements of Microaccelerations of ESA's Communication Satellite OLYMPUS," *Free-Space Laser Communication Technologies II, Proceedings of the SPIE,* vol. 1218, 1990.

[7] C. Racho and A. Portillo, "Characterization and Design of Digital Pointing Subsystem for Optical Communication Demonstrator," *Free-Space Laser Communication Technologies XI, Proceedings of the SPIE,* vol. 3615, no. 15, San Jose, January 1999.